Heliyon 9 (2023) e21349

Contents lists available at ScienceDirect

Heliyon

journal homepage: www.cell.com/heliyon

Synthesis and performance analysis of zeolitic imidazolate frameworks for CO_2 sensing applications

Shamma Al Abdulla [a], Rana Sabouni [b,*], Mehdi Ghommem [a], Abdul Hai Alami [c]

[a] Department of Mechanical Engineering, American University of Sharjah, Sharjah, 26666, United Arab Emirates
[b] Department of Chemical and Biological Engineering, American University of Sharjah, Sharjah, 26666, United Arab Emirates
[c] Department of Sustainable and Renewable Energy Engineering, University of Sharjah, United Arab Emirates

ARTICLE INFO

Keywords:
CO_2 detection
MOFs
Ball milling
Fluorescence intensity
Limit of detection
Selectivity

ABSTRACT

In this paper, we investigate the potential use of Zeolitic Imidazolate Frameworks (ZIF-8) as a sensing material for CO_2 detection. Three synthesis techniques are considered for the preparation of ZIF-8, namely room temperature, microwave-assisted, and ball milling. The latter is a green and facile alternative for synthesis with its solvent-free, room-temperature operation. In addition, ball milling produces ZIF-8 samples with superior CO2 adsorption and detection characteristics, as concluded from fluorescence measurements. Characterization tests including X-ray diffraction (XRD), Fourier transform infrared (FTIR), Thermogravimetric analysis (TGA), Field emission scanning electron microscopy (FE-SEM) and Energy-dispersive X-ray spectroscopy (EDS) are conducted to inspect the structural morphology, the thermal stability, and elements content of the ZIF-8 samples obtained from the different aforementioned synthesis techniques. The characterization tests revealed the appearance of a new phase of ZIF-8 which is ZIF-L when deploying the ball milling technique with different structure, morphology, response to CO_2 exposure and thermal stability when compared to its counterparts. Fluorescence measurements are carried out to evaluate the limit of detection (LOD), selectivity, and recyclability of the different ZIF-8 samples. The LOD of the ZIF-8 sample synthesized based on ball milling synthesis technique is 815.2 ppm, while LODs of the samples obtained from microwave and room temperature-based synthesis techniques are 1780.6 ppm and 723.8 ppm, respectively. This indicates that the room temperature and ball milling produced MOFs have comparable LODs. However, the room temperature procedure requires the use of a harmful solvent. The range of LOD demonstrates the suitable use of ZIF-8 for indoor air quality monitoring and other industrial applications.

1. Introduction

Accumulation of foreign materials in respiratory systems of living organisms is correlated with emissions caused by rapid industrial and transportation proliferation [1]. In particular, indoor air quality is a serious concern for inhabitants throughout the world as more and more of their time is spent indoors [2]. Many research studies support the idea that indoor air is more lethal than outdoor air [1]. As a result, gases such as NO2, SO2, and CO2, as well as NH3, are posing serious risks to public health [3]. The rising concentration of carbon dioxide (CO_2) indoors has been shown to affect human well-being and causes different diseases and shortness of breath. The

* Corresponding author. Department of Chemical and Biological Engineering, American University of Sharjah, Sharjah, 26666, United Arab Emirates.
E-mail address: rsabouni@aus.edu (R. Sabouni).

https://doi.org/10.1016/j.heliyon.2023.e21349
Received 22 June 2023; Received in revised form 7 October 2023; Accepted 19 October 2023
Available online 20 October 2023

indoor levels can reach above 1000 ppm with more building occupants and rapidly deteriorating ventilation conditions [4]. Current research has found that exposure to CO_2 at levels ranging from 500 to 4000 ppm results in linear rises in pCO_2 in the blood. Additional physiological indicators corresponding with higher sympathetic stimulation are reported in these investigations, such as changes in heart rate fluctuations and rises in circulation of the peripheral blood at CO_2 levels from 500 to 4000 ppm [5]. Enclosed spaces are subject to CO_2 buildup, which can displace oxygen. The expression "confined space hypoxic syndrome" was initially suggested for describing confined space incidents caused by oxygen-deficient environments that take place in water meter pits, vessels, ships' holds, mines, basement storage bins, and other similar environments [6]. While increased carbon dioxide concentrations in the atmosphere are a major global concern, most of us give little to no thought to the dangers caused by variations in CO_2 indoors [7]. Various sensors have been investigated, their working mechanisms rely on different principles, such as optical absorption, electrical resistance, field-effect transistors, and amperometry. Several conventional techniques, including electrochemical, infrared spectroscopic, GC-MS, and field-effect transistors, were utilized for CO_2 detection [8]. However, there are several challenges concerning the available CO_2 sensors, including the high cost, massive weight and large size [9]. It's also important to take into account the design of high performance materials for CO_2 detection [10]. Metal-oxide-semiconductor (MOS) based sensors have been recently used for gas detection but additional improvements in the sensing characteristics are needed to meet the needs of specific applications based on medical diagnosis, gas detection, etc., where high selectivity, low power consumption, quick response, low reliability on humidity, and a low limit of detection are required [11]. Hence, simple, inexpensive, and miniature sensors that work at severe conditions in nuclear reactors or oil wells are desirable [9].

Numerous studies have been focusing on different sensing techniques to create low-cost, low-power, and miniature sensors. To increase the sensitivity and selectivity of gas sensors, more studies should develop the modeling of gas sensors, material selection for sensing films, sensing layer morphologies, and other varied factors [12]. Several luminescence-based chemical sensors have been developed to date for the identification of particular chemical pollutants based on host-guest interactions, leading in the sensing of the desired molecules as low as the nanometer size range. Sensors composed of metal-organic frameworks (MOFs) materials are more appealing among these luminescence-based sensors because of their structural characteristics, functional content, and interactions between MOFs and analytes [13].

Metal-organic frameworks (MOFs), formed by joining metal clusters with organic linkers, exhibit a wide surface area which makes them desirable for various applications including utilization in gas sensing applications that require the gas analyte to be adsorbed within their structure, improving the selectivity of a gas sensor [14]. Through mass or mechanical changes utilizing microcantilevers and/or microresonators, spectroscopic measurements, changes in electric characteristics, calorimetry, and color change, the gas detecting response from the sensing layers can be quantified [15]. MOFs have been extensively investigated for CO_2 capture and storage. However, the applicability of MOFs for CO_2 sensing is far less understood, and only a small number of research has been conducted. Different MOF structures can be constructed in order to attain high CO_2 selectivity [16]. Few studies have reported the employment of MOFs for CO_2 sensing and identified their limit of detection [16]. For instance, Wang et al. reported a limit of detection of 20 ppm for CO_2 when using near-infrared (NIR) optical fiber coated with HKUST-1 [17]. Additionally, Huang et al. developed an enhanced Raman scattering (SERS) based sensor with ZIF-8 MOF films that resulted in a LOD of 5×10^{-8} M with an 8 min response time [7]. The synthesis technique influences the structure, characteristics, and performance of MOFs [3]. The initial synthesis method was solvothermal. To create the MOF crystals, it entails dissolving metal precursors and organic linkers and putting them in a controlled reaction vessel. The temperature is typically kept below 220 °C during synthesis, and crystallization can take anywhere from a few hours to days [3].

Mechanochemical synthesis, which avoids the use of hazardous solvents, high temperatures, and/or corrosive catalysts used in conventional synthesis processes, has recently been proposed as an option for synthesizing MOFs [18]. The mechanochemical processes produced by ball milling or grinding are thought to be a clean, effective, and fast method with a high production rate (in kg/h) [19]. Although there have been tremendous improvements in synthesis techniques, the mechanism of mechanochemical processes is still not entirely understood. Applying constant mechanical stress has so far been discovered to be the cause of unexpected reactivity that cannot be explained by using classical chemistry [19]. Since the ball milling method for MOF synthesis includes fast reaction times, and eco-friendly conditions (such as room temperature and solvent-free), the reduced carbon economy can be strengthened by incorporating ball-milled MOFs with gas sensing technologies. Zeolitic imidazolate frameworks, such as ZIF-8, have shown outstanding promise for CO_2 capture. Altering their structure by transferring some of their component organic ligands is an established technique for increasing the capacity for CO_2 absorption [20]. In light of this, the creation of ball-milled ZIF-8 facilitates the CO_2 detection and help in achieving Sustainable Development Goals (SDGs). The process of creating chemical molecules in a sustainable manner is known as "green chemistry." Green chemistry seeks to reduce the harmful impact that the synthesis of diverse chemical products has on the environment. The entire process of producing the nanomaterials can be done using green chemistry [21].

The objective of this work is to develop a novel and environmentally conscious pathway of synthesizing ZIF-8 and assess its potential for CO_2 sensing applications. The present study presents a significant contribution to the field by introducing innovative aspects in the synthesis and assessment of ZIF-8. We address the need for facile, energy-efficient and environmentally friendly synthesis method for ZIF-8. To achieve this, three different synthesis techniques, namely room temperature, microwave-assisted, and ball milling were employed. The ball-milling technique stands out as a green alternative, offering enhanced sustainability in MOF synthesis. The other synthesis methods described in the literature, including sonochemical, electrochemical, and slow diffusion, either require the use of sufficient solvents or a longer time for synthesis. Fluorescence measurements are conducted to evaluate the limit of detection, the selectivity and recyclability of ZIF-8. Through our research, we aim to explore new directions and potentials of ZIF-8 as a fluorescent probe for rapid and sensitive detection of CO_2 in competitive environment of other gases. By integrating innovative synthesis techniques and characterizing the performance of ZIF-8, we contribute to advancing the field of gas detection and emphasize

the importance of sustainability and safety in industrial settings. The exposure to hazardous gases from industrial operations, such as carbon monoxide (CO), carbon dioxide (CO_2), and methane (CH_4), can result in fatal incidents and serious injury to humans. Deploying gas detectors with the capability to identify the possible hazards posed by these gases is therefore essential to prevent their spread and the pain or damage they may cause to the working environment.

2. Experimental methods

2.1. Materials

The gases used for the experiments are Argon (99.998%), CO_2 (99%), and Nitrogen (99.998%) which were obtained from Caltrols Middle East LLC. All Chemicals were obtained from LabCo, the local supplier for Sigma Aldrich in the UAE and used without any further modification. The materials include zinc nitrate hexahydrate ($Zn(NO_3)_2{\cdot}6H_2O$, 99%), 2-methylimidazole ($CH_3C_3H_2N_2H$, 99%), and dimethylformamide (DMF). The preparation of the MOF takes three main routes: (i) microwave-assisted (S1), (ii) room temperature (S2) and (iii) mechanical ball milling (S3) approaches. These will be detailed in the following sections.

2.2. Synthesis of ZIF-8 using microwave-assisted procedure (S1)

The previously described method by Hillman [22] was used for the microwave synthesis with the modest modification of doubling the amount of materials. In 15 mL of methanol, 0.65 g of zinc nitrate hexahydrate was dissolved. Then, 15 mL of methanol was also used to dissolve 0.73 g of 2-methylimidazole. The resultant solution was then put into a 50 mL Teflon-lined microwave reaction vessel that was designated for microwave irradiation and microwaved using the laboratory Microwave of the model MDS-6G Digestion, obtained from a Chinese manufacturer of Laboratory equipment, Sineo, for 90 s at 100 W. After that, it was centrifuged, washed three times with methanol, and overnight dried in an oven at 80 °C.

2.3. Synthesis of ZIF-8 using room temperature procedure (S2)

The synthesis was carried out in accordance with the previously published method by Hunter-Sellars et al. [23], in which 1.642 g of 2-methylimidazole was dissolved in 50 mL of methanol and combined with 0.745 g of zinc nitrate hexahydrate dissolved in 50 mL of methanol. After being centrifuged and thoroughly washed with methanol three times, the precipitate was dried under vacuum for the next 24 h at room temperature.

2.4. Synthesis of ZIF-8 using ball milling (S3)

The Pulverisette 7 planetary ball mill from Fritsch's premium line was used to synthesize the MOF using ball milling. The amount of ligand and metal cluster were obtained from Zhang et al. earlier work [24], although the synthesis method was modified without the addition of solvents. Two 7 mm diameter stainless steel balls were added in the ball mill with 1.484 g of $Zn(NO_3)_2{\cdot}6H_2O$ and 3.278 g of Hmim for an hour. The ball mill was run at its maximum speed of 1100 rpm. After that, the sample was centrifuged. The created milky dough was washed with methanol and dimethylformamide (DMF) to get rid of any remaining metal ions and ligands. Subsequently, the sample was dried for 4 h at 100 °C in the oven.

2.5. Characterization

For all the resultant MOFs, 5 mg were used for characterization before and after exposing to CO_2 for 5 min. The Bruker D8 Advance DaVinci multifunctional X-ray diffractometer with Cu K radiation operating at $\lambda = 1.5406A^{\circ}$, 40 kV tube voltage, and 40 mA current was used for the X-Ray Diffraction (XRD) test. The range of 5.0°–40.0° with a step size of five, is where the XRD patterns are captured at $\Delta\theta = 25$ °C. TESCAN's VEGA3 XM is used for EDS analysis which runs at 5 kV operating voltage for both map and point modes. The FE-SEM analysis was done using JEOL JSM-7500F FESEM at 3 kV. TGA-50 Series from SHIMADZU was used for thermogravimetric analysis under temperature range from 25 °C to 800 °C with heating rate of 5 °C/min. FTIR analysis was conducted using JASCO FT/IR-

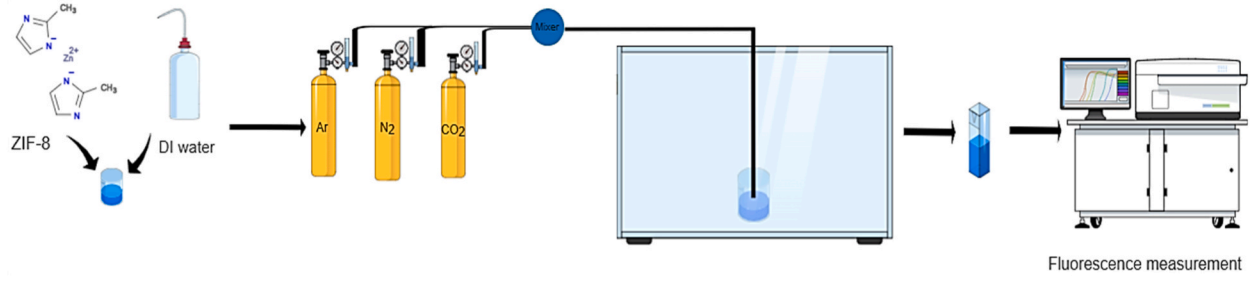

Fig. 1. Illustrative schematic of the procedure used for fluorescence measurements.

6300 Fourier transform infrared spectrometer in the range (4000-400 cm^{-1}) to identify the chemical composition and physical state of the samples. Surface area and adsorption-desorption isotherms were performed using Autosorb iQ utilizing multipoint Brunauer Emmett Teller (BET) method. The pore volume was reported using density functional theory (DFT) method. Samples were degassed under vacuum at 150 °C for 15.4 h.

2.6. Experimental procedure for CO_2 detection, selectivity and regeneration

The DW-F97Pro Fluorescence Spectrophotometer obtained from Drawell was used to test the fluorescence intensity (as shown in Fig. 1) of the prepared ZIF-8 suspension before and after exposure to CO_2. A suspension of the fluorescent probe (ZIF-8) of 100 mg/L was prepared by sonicating 5 mg of the ZIF-8 in 50 mL of deionized for 15 min to ensure full suspension of the MOF particles. Then, 3 mL of the mixture was taken for fluorescence measurement at 300–600 nm using excitation wavelength of 240 nm. The baseline before CO_2 exposure was recorded for each synthesized MOF. The detection measurements were performed through bubbling CO_2 into 3 mL of the MOF suspensions at different concentrations for 20 s. The experimental set-up is shown in Fig. 2 (a)-(b). The fluorescence efficiency was obtained using Equation (1):

$$Fluorescence\ Quenching\ Efficiency\ \% = \frac{I_{immediate}}{I_{baseline}} \times 100 \tag{1}$$

where $I_{baseline}$ is the initial intensity of the MOF with water before exposing it to the analyte, and $I_{immediate}$ is the fluorescence intensity after exposing the MOF to the gas analyte [25].

A series of tests were run to assess the performance of the three MOFs in various controlled environments. The MOFs were first examined with CO_2 bubbled by a gas cylinder. Using high-resolution mass-flow controller obtained from Caltrols Middle East LLC, the amount of the gas was increased. In each case, the three trials were averaged and the standard error was taken. The selectivity experiments were conducted in which other gases including N2, Ar and air were compared to CO_2 by measuring the fluorescence intensity at a fixed flow rate of 0.15 L/min. Finally, the regeneration experiments were conducted to investigate the recyclability of the MOF and its capability to maintain a good detection level of CO_2 by observing the quenching and recovery of the fluorescence intensity upon the injection of CO_2 and N_2, respectively. The regeneration experiments were performed for 3 cycles.

3. Results and discussion

3.1. Characterization tests

3.1.1. XRD analysis

The XRD patterns of the ZIF-8 samples prepared using the three different synthesis techniques, before and after exposure to CO_2 are shown in Fig. 3. The crystal structure of the three synthesized MOFs are in close agreement with previous studies and confirm the phase purity [26]. The XRD patterns of the MOFs obtained from S1 and S2 indicate the sodalite structure of the material [26,27] with sharp peaks at 2θ of 7.30°, 10.35°, 12.70°, 14.80°, 16.40° and 18.00° [28]. An alteration in the structure after adsorption of CO_2 is observed.

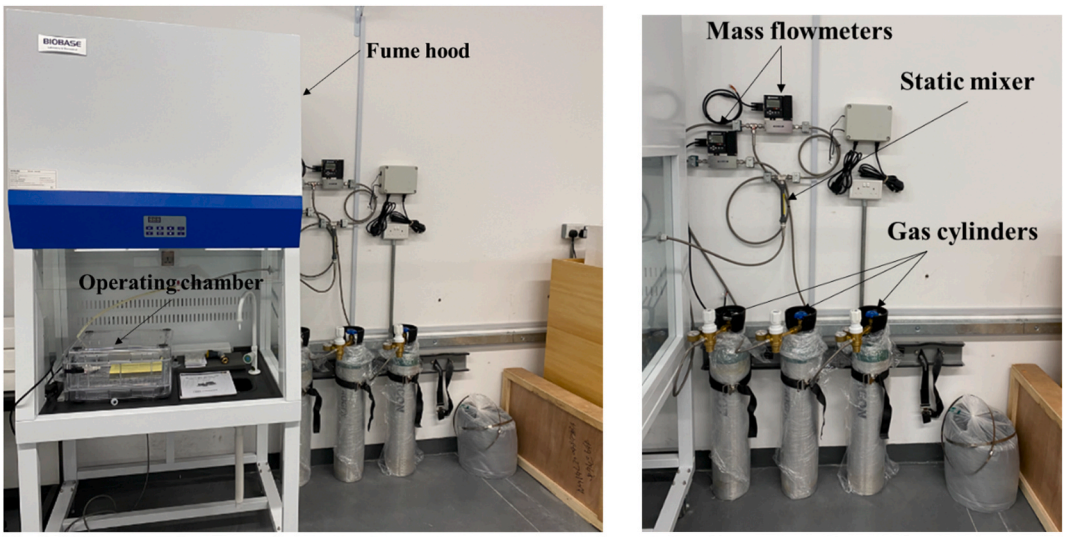

Fig. 2. Gas sensing apparatus: (a) The entire experimental set-up and (b) gas injection control unit.

For the MOF produced from S3, the XRD pattern reveals a 2D phase structure of ZIF-8, also known as ZIF-L with high crystallinity [27], especially with sharp peaks at 2θ of 7.58°, 10.80°, 12.54°, 14.95°, 16.49° and 17.86° [29]. For all the samples, the sharp and narrow peaks are indicative of the favorable crystallinity of the material. The variations in the XRD patterns of the ZIF-8 samples obtained from S1 and S2 upon exposure to CO_2 show that significant structural changes have emerged as a result of the attachment of the gas molecules, supporting the fact that a new arrangement has created and caused the formation of a second configuration composed of a CO2 molecule within the same crystallographic locations. The detection of the CO_2 species by XRD from the increased intensity indicates the presence of small chemisorbed species that results from chemical bonds such as the π … π interaction between CO_2 and aromatic rings of the linker [30]. As for the ZIF-8 sample obtained from S3, there is no notable difference in the XRD patterns after exposure to CO_2 which can indicate that the CO2 species are only physisorbed [31]. In the ZIF-8 and ZIF-L cages, the diameter of the six-membered ring's aperture where the methyl groups of the linker are pointing to the center allows the diffusion of CO_2 into the pores. The physisorbed interactions occur by the favorable electrostatic adsorption sites which are located on both edges of six-ring channel and in the center of the available surface area near to the aromatic rings, in addition to the van der Waals interactions that are high in the sodalite cage [32].

3.1.2. FE-SEM/EDS analysis

Fig. 4(a)-(f) show the FE-SEM images obtained for the different ZIF-8 samples (S1, S2, and S3). The synthesis approach worked because the ZIF-8 crystals resulted from the S1 and S2 synthesis had rhombic dodecahedron morphologies, which is in agreement with the results found in literature [26]. On the other hand, the ZIF-L 2D phase obtained from S3 had a closer morphology to a cruciate flower, which also confirms the results found in Ref. [27]. It can also be observed that there is no major difference in the morphology after adsorption of CO_2. The EDS color map in Fig. 5(a)-(f) show the elemental composition of each sample (S1, S2, and S3) before and after CO_2 exposure. The mapping revealed that the C, Zn, and N elements were distributed uniformly on the surface of the MOFs. The O element could be obtained from the zinc nitrate hexahydrate residue or the conductive sticky substrate employed in the characterization [26]. The percentage of C in all the samples increased after exposure to CO_2, and thus, confirms the CO_2 capture. Furthermore, in Fig. 5(f), the reaction of Zn with CO_2 leads to the production of ZnO. The surface area of ZnO per Zn amount rises as the uniform mix of Zn powder and ZnO's mass fraction increases, in addition to the increase in Zn particles' degree of dispersion [33]. Hence, this could be one of the reasons explaining the reduction in Zn wt% and increase in O_2 and N_2. According to literature [34], CO_2 uptake within the microstructure causes the depletion of the zinc, more Zn would be depleted from the microstructure or it formed as a thin surface ZnO film that will not be detected with EDS, which could explain the lower values in the EDS measurements (from ~42 % to 1.6 %).

3.1.3. FTIR spectroscopy analysis

Fig. 6 displays the Fourier transform infrared (FTIR) spectra of the ZIF-8 samples. The FTIR results demonstrate that ZIF-8 successfully incorporated amino groups. For the ZIF-8 samples (S1 and S2), notable bands are obtained at 2926, 1458, 1425, 1385, 1309, 1146, 995, 760, 694, and 426 cm^{-1}. These FT-IR bands are in close agreement with those previously reported in Refs. [18,19].

For the ZIF-L phase (S3 sample), the following peak designations are made: 1570 cm^{-1},C = N stretching; 755 cm^{-1}, Zn–O imidazole

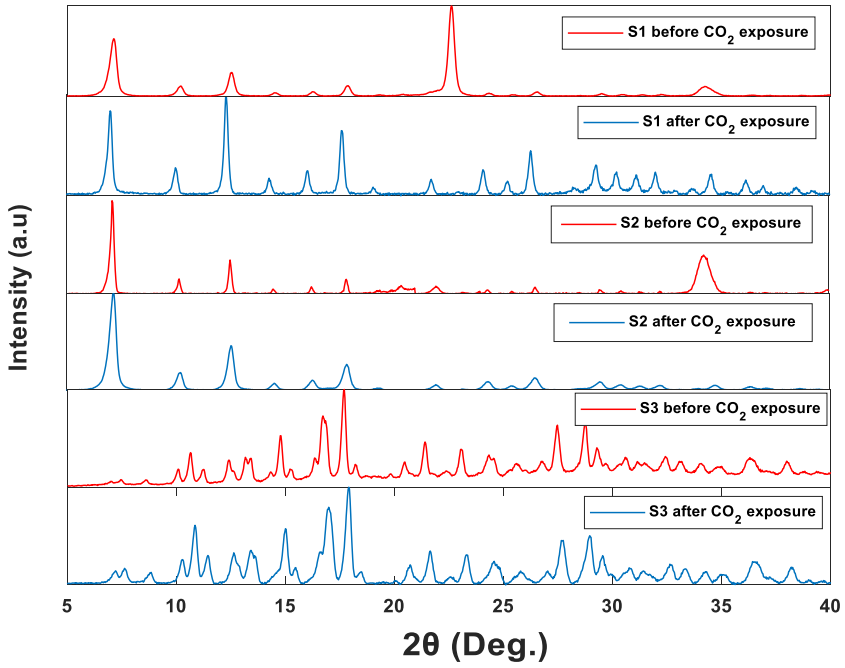

Fig. 3. XRD patterns for S1, S2, and S3 MOFs before and after CO_2 exposure.

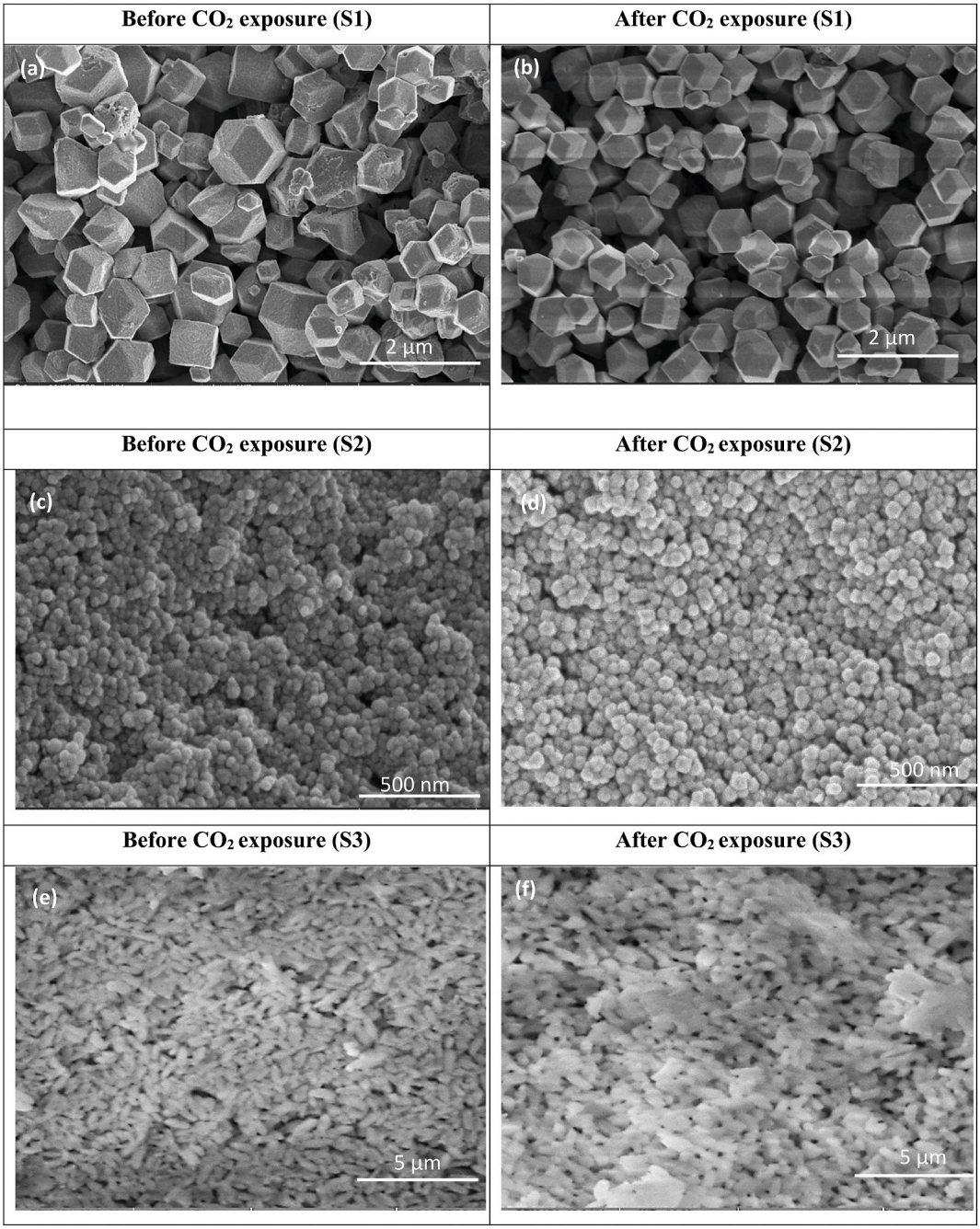

Fig. 4. FE-SEM for ZIF-8 synthesized using (a) S1 before CO_2 exposure, (b) S1 after CO_2 exposure, (c) S2 before CO_2 exposure, (d) S2 after CO_2 exposure and (e) S3 before CO_2 exposure, (f) S3 after CO_2 exposure.

ring bending; 674 cm^{-1}, Zn–N imidazole ring bending. The spectrum after adsorption of CO_2 not only confirms the storage of CO_2, but it also offers compelling proof of CO_2 and ZIF-8 framework interactions. For example, the 1146 cm^{-1} generated from the aromatic C–N stretching mode, shows a sharper peak after adsorption of CO_2 in ZIF-8. Also, the bands between 1707 and 1366 cm^{-1} increased slightly due to the chemisorbed CO_2 in the ZIF-8 samples [31]. This is as opposed to the ZIF-L phase in which the peaks did not increase.

3.1.4. BET analysis

The N_2 adsorption-desorption isotherms for the ZIF-8 samples are shown in Fig. 7 at 77 K. The ZIF-8 samples produced from the S1 and S2 synthesis obviously exhibited type I isotherm behavior, indicating that they are micropores. These results are consistent with previously reported ZIF-8 isotherms [18]. Furthermore, at low (P/P_0) pressures, the adsorbed nitrogen in all samples rises steadily,

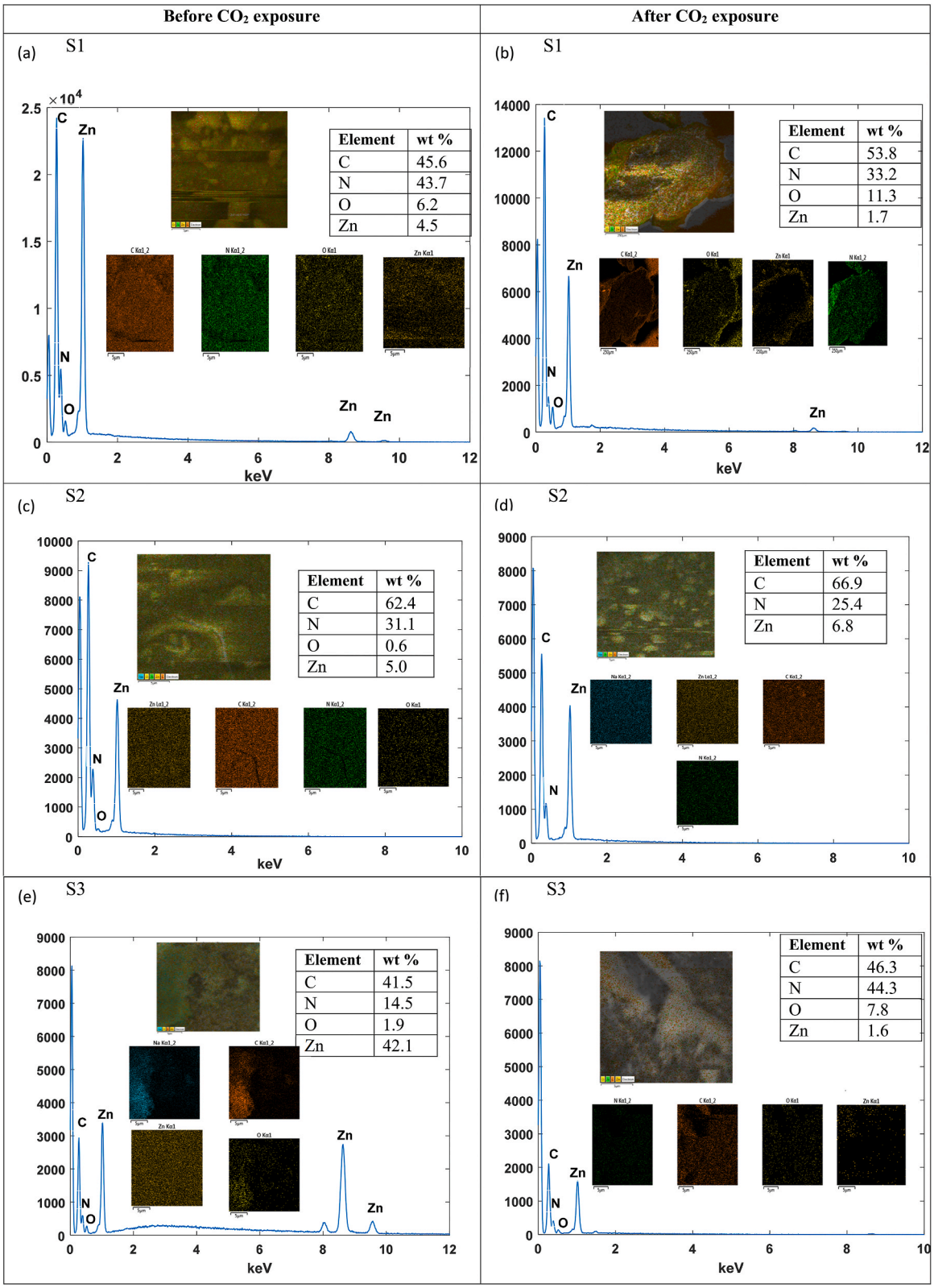

Fig. 5. EDS color map of (a) S1before CO_2 exposure, (b) S1 after CO_2 exposure, (c) S2 before CO_2 exposure, (d) S2 after CO_2 exposure, (e) S3 before CO_2 exposure, (f) S3 after CO_2 exposure.

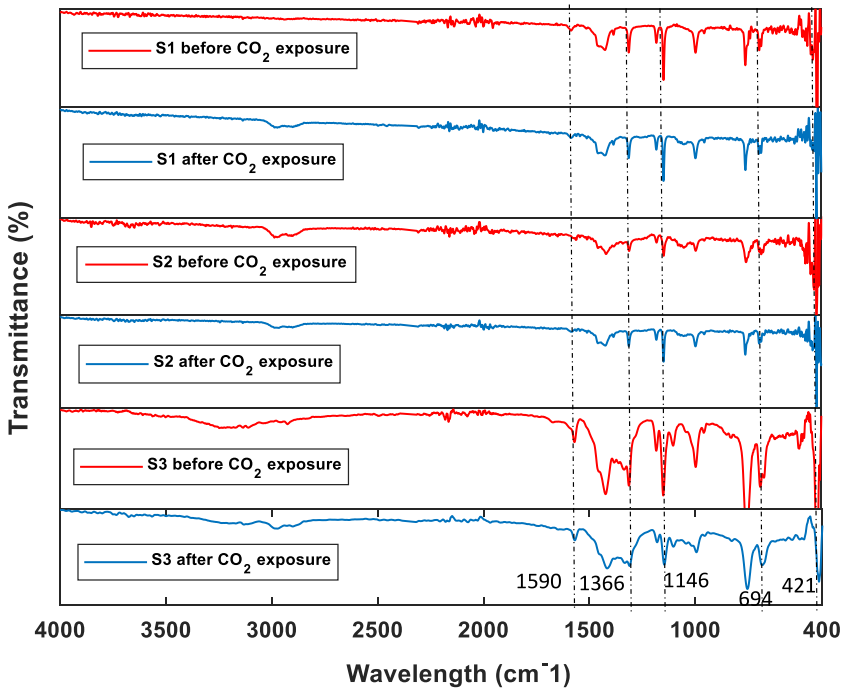

Fig. 6. FT-IR spectra for ZIF-8 samples before and after CO_2 exposure.

indicating the presence of micropores. On the other hand, the isotherm of ZIF-L sample obtained from S3 indicates type IV behavior. It constitutes then a mesopores material. In addition, the produced isotherms showed a hysteresis loop when approaching $P/P_0 = 1$. This demonstrates the existence of interfacial mesoporosity and macroporosity between MOF particles. The results are in agreement with the findings reported in Refs. [18,19]. The Brunauer–Emmett–Teller (BET) surface area and pore volume are shown in Table 1 before and after CO_2 exposure. It can be observed that the ZIF-8 samples obtained following S1 and S2 have much higher surface area and pore volume compared to the S3 sample. In fact, the ball milling high rotational speed reduced the surface area and due to the emergence of the ZIF-L phase, that have dense laminar structure, a lower surface area has resulted [35,36]. The reduction in both the surface area and pore volume after exposure to CO_2 proves the existence of CO_2 molecules within the material [37].

3.1.5. TGA analysis

We show in Fig. 8 the TGA results in terms of the variations of the mass percentage with the temperature. The results demonstrate the high thermal stability of all synthesized ZIF-8 samples. Furthermore, the observed trends are in close agreement with those obtained in Ref. [38]. For the S1 synthesized ZIF-8 (see Fig. 8(a)), an initial weight loss of about 1 % that occurred at about 200 °C, is mainly due to the methanol solvent evaporation. When reaching 400 °C, the greatest weight loss is observed. There was a 67 % weight loss that is mainly caused by the loss of organic linker molecules, leading to the destruction of the framework and the loss of certain species from the nanocrystals [39]. The TGA pattern of the S2 ZIF-8 (see Fig. 8(b)) showed that higher temperatures are needed for degradation, and thus, indicates a higher thermal stability. The initial reduction of 14 % occurred due to evaporation of trapped solvent, which was also methanol. This is followed by about 66 % of weight loss around 600 °C which results from the thermal decomposition of the MOF and organic linker dissociation.

As shown in Fig. 8(c), the TGA results of S3 synthesized ZIF-8 which corresponds to ZIF-L show a slightly different different trend from that of ZIF-8 obtained from S1 and S2. The weight loss occurs in two stages. In the first stage, the moisture evaporates within a temperature range from 50 °C to 300 °C. A weight loss of ~22 % with steeper slope initiates at 150 °C and continues until 300 °C. Beyond this temperature, the TGA curve shows a dramatic weight loss of about 56 % until reaching a temperature of 700 °C. This is caused by the thermal decomposition of ZIF-8, which takes place when 2-MIM breaks down at a high temperature and produces ZnO as the final decomposition byproduct of the nanocrystals. The TGA results demonstrate that the MOF structure was maintained in the ZIF-8 produced using the solvent-free technique up to 300 °C, which indicates a good thermal stability.

3.2. CO_2 detection tests

To assess the capability of ZIF-8 to detect CO_2, the response of the MOFs toward CO_2 is examined using the fluorescence method, as described in the previous section. The fluorescence materials have gained high interest in scientific investigations given their various prospective applications including sensing [40]. Fig. 9(a)-(f) show the fluorescence intensity as a function of the wavelength and the normalized intensity as function of the CO_2 concentration. The results are obtained based on the fluorescence measurements conducted

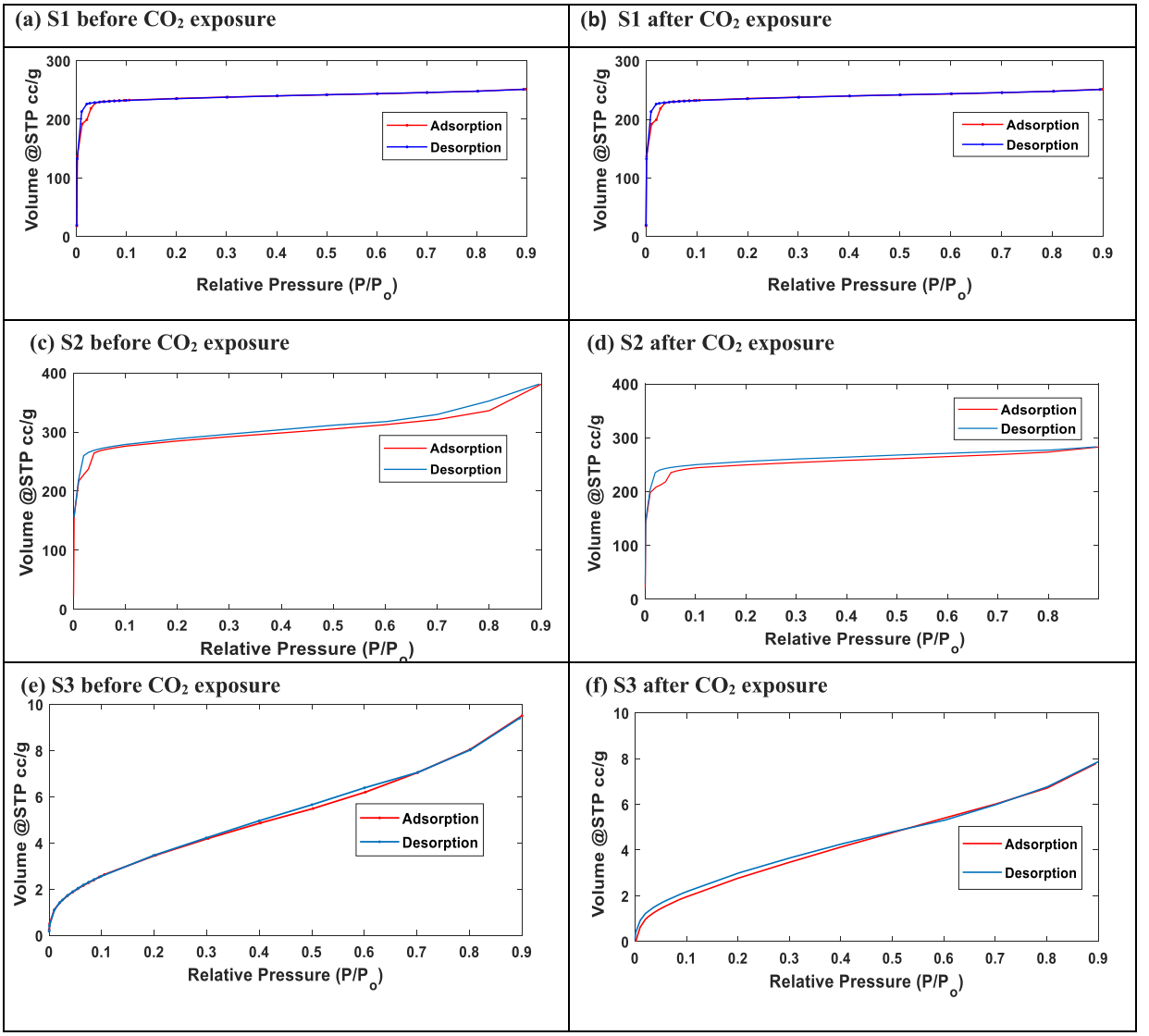

Fig. 7. Adsorption isotherms of ZIF-8 synthesized using (a) S1 before CO_2 exposure, (b) S1 after CO_2 exposure, (c) S2 before CO_2 exposure, (d) S2 after CO_2 exposure, (e) S3 before CO_2 exposure, (f) S3 after CO_2 exposure.

Table 1
Surface area, pore volume and pore diameter for the 3 samples before and after CO_2 adsorption.

Type	Experiment (before/after CO_2)	BET surface area (m^2/g)	Pore volume (cc/g)	Pore diameter (Å)
S1	Before	1084.614	0.373	13.7
	After	974.539	0.343	14.07
S2	Before	1136.505	0.527	18.5
	After	985.471	0.389	15.8
S3	Before	13.974	0.013	37.2
	After	12.199	0.011	36

on the ZIF-8 samples produced from S1, S2 and S3 synthesis techniques. For the samples obtained from S3 and S1, a reduction in intensity is observed after bubbling the CO_2 which indicates that the MOF exhibited a turn-off response, also known as quenching. There was a significant fluorescence quenching in the S3 sample after the injection of CO_2. The fluorescence intensity reduces dramatically from the baseline after bubbling with the highest gas concentration. This results in a quenching percentage of 93.42 %. The fluorescence intensity reduces as the concentration of the injected CO_2 increases until reaching saturation of 12.19 a. u. at a CO_2 concentration of 5.67×10^{-3} mol. This rapid and intense quenching reveals the capability of ZIF-8 to detect the CO_2 gas. The

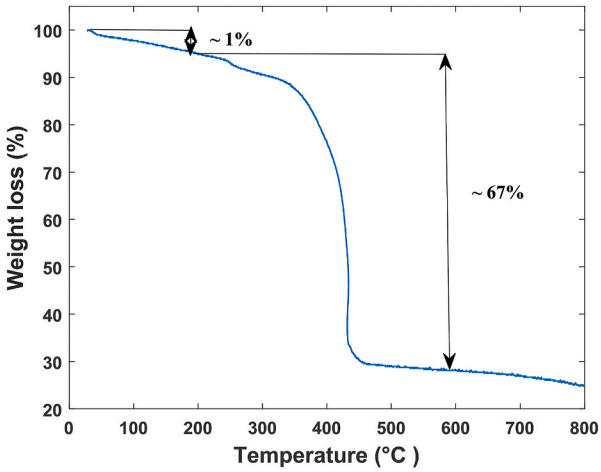

(a) S1 ZIF-8 sample

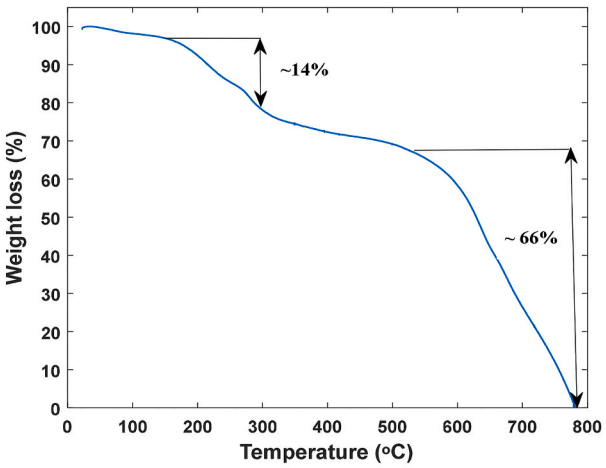

(b) S2 ZIF-8 sample

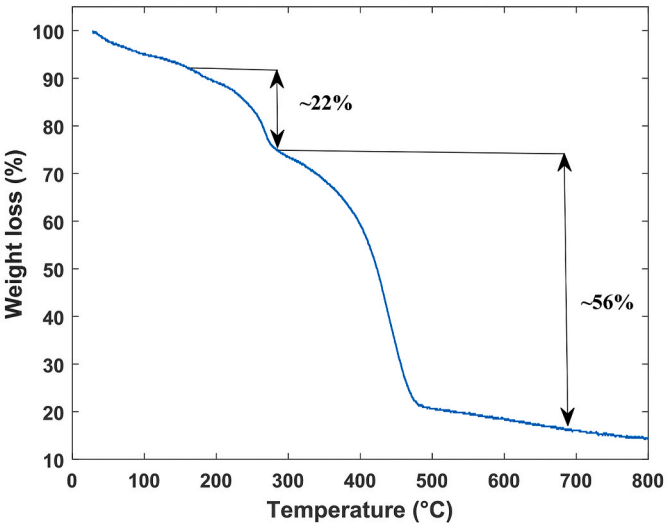

(c) S3 ZIF-8 sample

Fig. 8. TGA results of (a) S1, (b) S2, and (c) S3 ZIF-8.

fluorescence level can be used as an indicator of the presence of CO_2 and the associated concentration can be extracted from the fluorescence intensity. Moreover, the considerable reduction in the peak indicates that the CO_2 adsorption mechanism has a significant impact on the MOF luminescence characteristic, and the adsorption of the CO_2 molecules results in a major modification in the MOF structure. In these MOFs, the luminescence is dependent on the luminescence of the linker (2-methylimidazole), which is related to the π – interactions [41]. Since the most highly adsorptive sites for CO_2 in ZIF-8 and ZIF-L are those near the imidazole rings, the fluorescence is quenched upon interaction with CO_2 [32]. Another factor causing the quenching is the collisions due to interactions with the gas molecules which causes the deactivation of the MOFs [40]. On the contrary, for the S2 samples, the MOF was turned on as the intensity was increasing until reaching saturation point. The turn-on phenomenon can be attributed to the ZIF-8's larger pore size in this sample and the desirable molecular physical interactions between CO_2 and the surface. This high capacity is most likely a result of the MOF's high crystallinity, surface area and micropore volume. All of these factors contributed to adsorption of the electrophile CO_2 via bonding with the metal sites [42]. The aggregation that occurs due to the restriction of the rotating organic groups' molecular motion upon activation is mostly the driving force for fluorescence enhancement [40]. The fluorescence characteristics of materials are influenced by the synthesis process and morphology. Fluorescent materials' properties can be intensified or diminished due to changes in bonding, energy, or electron transport methods when they interact with other molecules [40].

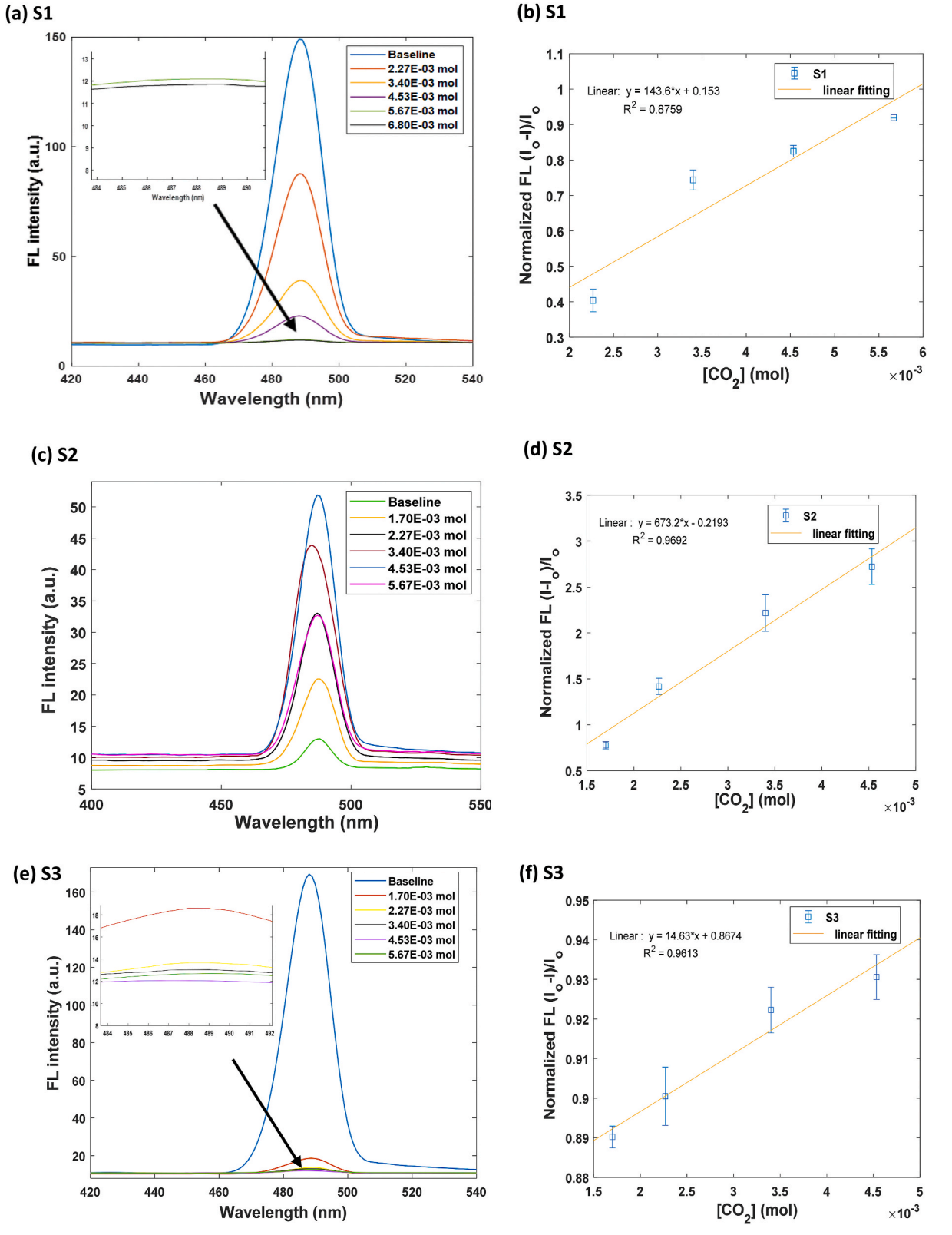

(caption on next page)

Fig. 9. Fluorescence intensity and Normalized Fluorescence of produced ZIF-8 samples: (a) S1 fluorescence intensity for different concentrations of CO_2, (b) S1 limit of detection, (c) S2 fluorescence intensity for different concentrations of CO_2, (d) S2 limit of detection and (e) S3 fluorescence intensity for different concentrations of CO_2, (f) S3 limit of detection. Points represent the average of three trials and error bars represent the standard deviation of three trials.

The linear relationship of the fluorescence intensity to CO_2 is found from 1.70 $\times 10^{-3}$ mol to 4.53 $\times 10^{-3}$ mol for the S3 (see Fig. 9 (f)) and S2 samples (see Fig. 9(d)), and 2.27 $\times 10^{-3}$ to 5.67 $\times 10^{-3}$ mol in the S1 sample (Fig. 9(b)). Also, there is a strong linear correlation in the plot of fluorescence intensity against CO_2 concentration in which the R^2 values were 0.8759, 0.9692, and 0.9613, for S1, S2 and S3 samples, respectively. The CO_2 adsorption occurs in the MOFs due to the high electronegativity of the functional groups [20]. Also, the open metal site displays a considerable interaction with CO_2 as a result to an electrophile of CO_2 [43].

The limit of detection was calculated using the calibration curve shown in Fig. 9 (b), (c) and (f). The linear equation was obtained by plotting the normalized fluorescence intensity (i.e. $\frac{I_0-I}{I_0}$, where I and I_o represent the fluorescence intensity with and without exposure to the analyte, respectively [44]) versus the concentration of CO_2. Furthermore, LOD was obtained using equation (2) below:

$$\mathrm{LOD} = \frac{3\sigma}{s} \tag{2}$$

where σ and s are the standard deviation of the baseline and the slope of the calibration curve (shown in Fig. 9 (b), (d) and (f)), respectively [45]. The S2 ZIF-8 shows the lowest limit of detection (723.8 ppm at 25 °C) while the S1 ZIF-8 sample yields the highest value of LOD (1780.6 ppm). This might be attributed to the use of a vacuum oven at room temperature for obtaining the resultant MOF which caused high crystallinity of the material. This was also observed in the XRD patterns where the main peaks related to the crystallinity of the material were higher for the S2 MOF and then, leading to an improvement in its CO_2 detection capability. The S3 MOF shows a good potential for CO_2 detection given the obtained LOD value of 815.2 ppm, and hence, proves the validity of the ZIF-L for CO_2 detection. In a previous study by Ref. [46], ZIF-8 was synthesized using the solvothermal technique and resulted in a LOD of 3130 ppm at room temperature and 774 ppm at 4.85 °C. The applications where our synthesized MOFs could be utilized are in indoor buildings at room temperature in addition to the industrial processes. Buildings typically have indoor air with a CO_2 concentration between 350 and 2500 ppm, according to ANSES [47]. Another study, dealing with benzene and CO_2 detection at room temperature, reported a sensor consisting of MOF films produced on-chip on Pt interdigitated electrodes using a solvothermal technique. The LOD of the adjusted Mg-MOF-74 tested for CO_2 detection was found equal to 200 ppm [15]. A recent study by Lee et al. [45], revealed that under optimal conditions, the LOD calculated for PVIm-NH_2 based chemosensor was 110 ppm.

Next, we examine the selectivity of the S3 MOF sample (ZIF-L) by inspecting the quenching of its fluorescence intensity when exposed to different gases, including N_2, Ar, and air. The selectivity results under room temperature are shown in Fig. 10. The results demonstrate that ZIF-L is more selective to CO_2. The ratio I/I_o where I is the intensity obtained after exposing the CO_2 with a concentration of 0.15 L/min to the MOF for 20 s and I_o is the baseline intensity reaches 18.34 %. Larger values of the ratio I/I_o are obtained for N_2, Ar, and air. Clearly, ZIF-L is much less sensitive to air. This is desired for applications where other competing gases exist. In the study of Chocarro-Ruiz et al. [46], a high selectivity over N_2 was obtained at low temperature. Since ZIF-L features a 9.4 °A × 7.0 °A × 5.3 °A cushion-shaped hollow between the layers that can accommodate CO_2 molecules. Similarly, the imidazole functional group on ZIF-L particles can interact strongly with CO_2 [48]. In fact, this type of MOF has the desired selectivity performance, because of its smaller pore size compared to S1 and S2 which is desirable for selective adsorption of CO_2 [49].

The quenching-recovery cycles were performed to test the recyclability of the S3 MOF sample. The corresponding results in terms of changes in the fluorescence intensity are shown in Fig. 11. After exposing it to CO_2, the fluorescence recovery is observed by bubbling N_2 and then the fluorescence quenching is observed again when exposing it again to CO_2 in which the MOF is able to regenerate. However, after the second cycle, the MOF lost its ability to regenerate most probably due to its degradation in water [49]. In Table 2, we show a comparison of different MOFs used for CO_2 detection.

The noticeable change in brightness when exposing ZIF-8 or any of its variants to CO_2 can be exploited to quantify the CO_2 concentration using hardware and software tools. The fluorescence intensity of sensing materials can be increased, quenched, or changed in color, and thus can be used for optical sensing devices. A high surface-volume ratio, which enables the detection of a low levels of target analytes, is a factor contributing to the advantages of utilizing optical nanoparticles [40]. The visual fluorescence color variation of the solution using UV light irradiation (365 nm), as shown in Fig. 12, clearly demonstrates the quenching phenomenon when increasing the flow rates of CO_2 from 0.15 L/min (1.70 $\times 10^{-3}$ mol) to 0.7 L/min (7.93 $\times 10^{-3}$ mol). The last case also shows the complete saturation of the MOF. It is also important to note that the change occurs immediately upon bubbling the CO_2.

4. Conclusion

In this paper, we demonstrated the capability of the MOF ZIF-L synthesized by the ball milling technique to detect CO_2 gas with an LOD of 815.2 ppm at room temperature, exhibiting high selectivity of other gases. In addition, the performance analysis of the MOFs obtained from other synthesis techniques were examined. The room temperature synthesized MOF showed an LOD of 723.8 ppm, which is lower than the ZIF-L phase. While the microwave synthesized MOF had a higher LOD of 1780.6 ppm. XRD characterizations showed the physisorption and chemisorption interactions with CO_2, while FTIR, FE-SEM and EDS tests revealed the differences in morphology and structure between the ZIF-8 and ZIF-L phase, before and after exposure to CO_2. The BET analysis showed the reduction in the pore size of the MOFs upon CO_2 adsorption. The findings demonstrate the following two important points: (i) the enormous

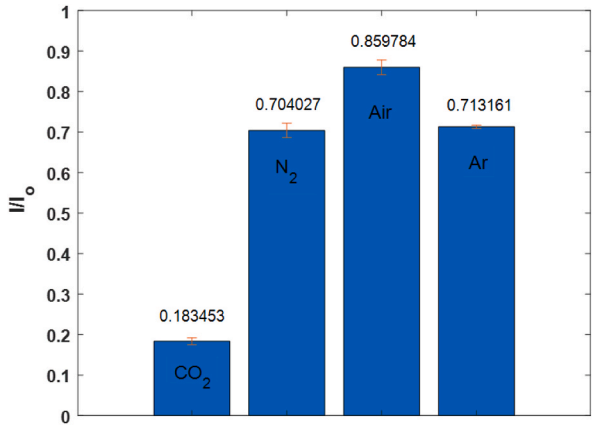

Fig. 10. Selectivity results of S3 MOF when exposed to CO_2 and other gases.

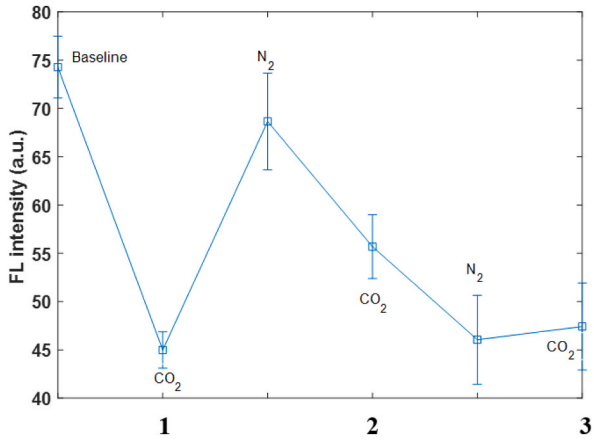

Fig. 11. Changes in the fluorescence intensity of the ZIF-8 (S3) upon exposure to CO_2 over three cycles.

Table 2
MOFs synthesized by different procedures and their corresponding characteristics for CO_2 sensing.

MOFs	Synthesis	CO2 capacity	CO2 selectivity	Limit of Detection	Reference
ZIF-8	–	–	High	5×10^{-8} M	[7]
Co(II)-MOF	Solvothermal	–	High	–	[50]
ZrFSIX-2-Zn-i	Solvothermal	4.56 mmol g^{-1}	High	–	[51]
Al-MIL-53 + conductive carbon	Solvothermal	–	High (over CH_4)	–	[52]
MIL-101(Cr, Mg)	Solvothermal	Reached 3.28 mmol/g at 298 K and 1 bar	High over N_2, enhanced up to 86 at 100 kPa	–	[53]
dmen-Mg_2(dobpdc) (dmen = N,N-dimethylethylenediamine)	Microwave	At 25 °C and 0.15 bar, 1-dmen takes up 3.77 mmol/g of CO_2	High over N_2.	–	[54]
Cd(II)	Solvothermal	CO_2 uptake is 27.5 cm^3 g^{-1} at 273 K and 1 bar	High over CH_4.	–	[55]
Cu-BTC	Solvothermal	–	–	500 ppm	[56]
MIL-101(Cr)	Hydrothermal	3.16 mmol/g	–	–	[57]
ZIF-8 nanoparticles	Solvothermal	Greater at lower temperature	Greater over N_2 at lower temperatures	3130 ppm at room temperature and 774 ppm at 278 K.	[46]

potential of mechanochemistry to develop an efficient and solvent-free MOF synthesis; and (ii) the necessity of further research into continuous, higher-scale mechanochemical processes, in order to increase the effectiveness and sustainability of the process. For future work, the material will be integrated with a MEMS device that detects the changes in mass after gas adsorption. The majority of reported CO_2 sensors require huge equipment to detect. As a result, we anticipate that more research will be conducted to evaluate the

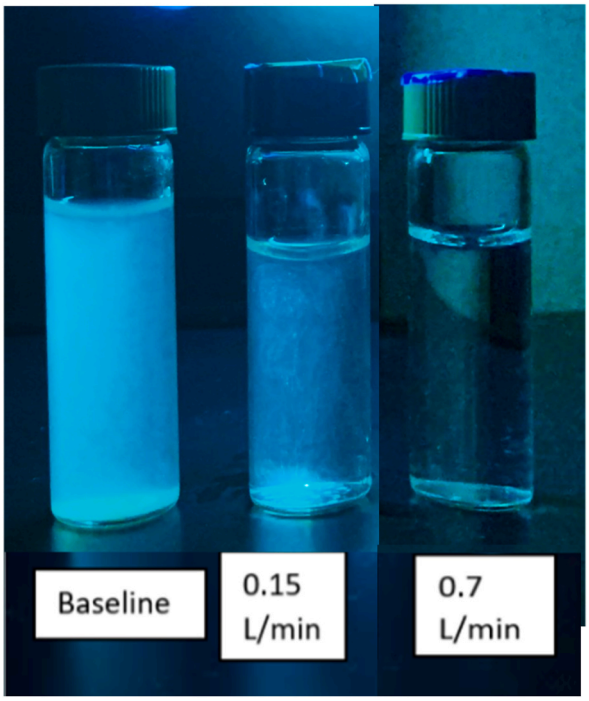

Fig. 12. MOFs' turn-off in the water after being bubbled with CO_2 at two different concentrations and exposed to UV light.

MOFs potential for miniature sensors. Furthermore, this MOF could be investigated for the detection of other toxic gases such as CO gas.

Data availability statement

Data will be made available on request.

CRediT authorship contribution statement

Shamma Al Abdulla: Writing – original draft, Investigation, Data curation. **Rana Sabouni:** Writing – review & editing, Supervision, Resources, Project administration, Methodology, Funding acquisition, Conceptualization. **Mehdi Ghommem:** Writing – review & editing, Supervision, Resources, Project administration, Funding acquisition. **Abdul Hai Alami:** Writing – review & editing, Resources.

Declaration of competing interest

The authors declare that they have no known competing financial interests or personal relationships that could have appeared to influence the work reported in this paper.

Acknowledgements

The study presented in the paper was financially supported via the faculty research grant from the American University of Sharjah (FRG21-*M*-E63), the Open Access Program from the American University of Sharjah (OAPCEN-1410-E00198) and the Sharjah Research Academy (SRA 223150). This paper represents the opinions of the author(s) and does not mean to represent the position or opinions of the American University of Sharjah.

References

[1] J. Saini, M. Dutta, G. Marques, A comprehensive review on indoor air quality monitoring systems for enhanced public health, Sustain. Environ. Res. 30 (6) (2020), https://doi.org/10.1186/s42834-020-0047-y.
[2] J.P. Sá, M.C.M. Alvim-Ferraz, F.G. Martins, S.I.V. Sousa, Application of the low-cost sensing technology for indoor air quality monitoring: a review, Environ. Technol. Innov. 28 (2022), 102551, https://doi.org/10.1016/j.eti.2022.102551.
[3] X. Chen, M. Leishman, D. Bagnall, N. Nasiri, Nanostructured gas sensors: from air quality and environmental monitoring to healthcare and medical applications, Nanomaterials 11 (8) (2021) 1927, https://doi.org/10.3390/nano11081927.

[4] A.K. Davey, et al., Amine-functionalized metal-organic framework ZIF-8 toward colorimetric CO2 sensing in indoor air environment, Sens. Actuators, B 344 (2021), 130313, https://doi.org/10.1016/j.snb.2021.130313.
[5] K. Azuma, N. Kagi, U. Yanagi, H. Osawa, Effects of low-level inhalation exposure to carbon dioxide in indoor environments: a short review on human health and psychomotor performance, Environ. Int. 121 (1) (2018) 51–56, https://doi.org/10.1016/j.envint.2018.08.059.
[6] K. Permentier, S. Vercammen, S. Soetaert, C. Schellemans, Carbon dioxide poisoning: a literature review of an often forgotten cause of intoxication in the emergency department, Int. J. Emerg. Med. 10 (14) (2017), https://doi.org/10.1186/s12245-017-0142-y.
[7] A. Gheorghe, O. Lugier, B. Ye, S. Tanase, Metal–organic framework based systems for CO 2 sensing," Journal of Materials Chemistry C. Royal Society of Chemistry (2021) 1–11, https://doi.org/10.1039/d1tc02249k.
[8] Y. Tang, et al., A highly fluorescent post-modified metal organic framework probe for selective, reversible and rapid carbon dioxide detection, Dyes Pigments 172 (2020), 107798, https://doi.org/10.1016/j.dyepig.2019.107798.
[9] M.Y. Rezk, J. Sharma, M.R. Gartia, Nanomaterial-based co2 sensors, Nanomaterials 10 (11) (2020) 2251, https://doi.org/10.3390/nano10112251.
[10] Y. Zheng, X. Xu, X. Zhang, L. Qin, Y. Lu, G. Zhang, Design of metal-organic frameworks with high lowpressure adsorption performance of CO2, in: IOP Conference Series: Earth and Environmental Science, 2018, 032073, https://doi.org/10.1088/1755-1315/170/3/032073.
[11] J. Zhang, Z. Qin, D. Zeng, C. Xie, Metal-oxide-semiconductor based gas sensors: screening, preparation, and integration, Phys. Chem. Chem. Phys. 19 (9) (2017) 6313–6329, https://doi.org/10.1039/c6cp07799d.
[12] H.R. Shwetha, S.M. Sharath, B. Guruprasad, S.B. Rudraswamy, MEMS based metal oxide semiconductor carbon dioxide gas sensor, Micro Nano Eng 16 (September 2021) (2022), 100156, https://doi.org/10.1016/j.mne.2022.100156.
[13] D. Zhao, et al., Recent progress in metal-organic framework based fluorescent sensors for hazardous materials detection, Molecules 27 (7) (2022) 1–34, https://doi.org/10.3390/molecules27072226.
[14] X. Chen, R. Behboodian, D. Bagnall, M. Taheri, N. Nasiri, Metal-organic-frameworks: low temperature gas sensing and air quality monitoring, Chemosensors 9 (2021) 316, https://doi.org/10.3390/chemosensors9110316.
[15] D.J. Wales, et al., Gas sensing using porous materials for automotive applications, Chem. Soc. Rev. 44 (2015) 4290–4321, https://doi.org/10.1039/c5cs00040h.
[16] B. Ye, A. Gheorghe, R. Van Hal, M. Zevenbergen, S. Tanase, CO2 sensing under ambient conditions using metal-organic frameworks, Mol. Syst. Des. Eng. 5 (6) (2020) 1071–1076, https://doi.org/10.1039/d0me00004c.
[17] X.S. Xing, Z.H. Fu, N.N. Zhang, X.Q. Yu, M.S. Wang, G.C. Guo, High proton conduction in an excellent water-stable gadolinium metal-organic framework, Chem. Commun. 55 (2019) 1241–1244, https://doi.org/10.1039/c8cc08700h.
[18] R. Zhang, C.A. Tao, R. Chen, L. Wu, X. Zou, J. Wang, Ultrafast synthesis of Ni-MOF in one minute by ball milling, Nanomaterials 8 (2018) 1067, https://doi.org/10.3390/NANO8121067.
[19] A.D. Katsenis, et al., In situ X-ray diffraction monitoring of a mechanochemical reaction reveals a unique topology metal-organic framework, Nat. Commun. 6 (2015) 6662, https://doi.org/10.1038/ncomms7662.
[20] Y.W. Abraha, C.W. Tsai, J.W.H. Niemantsverdriet, E.H.G. Langner, Optimized CO2Capture of the zeolitic imidazolate framework ZIF-8 modified by solvent-assisted ligand exchange, ACS Omega 6 (34) (2021) 21850–21860, https://doi.org/10.1021/acsomega.1c01130.
[21] S. Tiwari, S. Talreja, Green chemistry and microwave irradiation technique: a review, J. Pharm. Res. Int., no. May (2022) 74–79, https://doi.org/10.9734/jpri/2022/v34i39a36240.
[22] F. Hillman, Developing Microwave-Assisted Synthesis For Hybrid Zeoliticimidazolate Frameworks Deriving From Zif-8 For Tunable Gas Separations, 2019.
[23] E. Hunter-Sellars, P.A. Saenz-Cavazos, A.R. Houghton, S.R. McIntyre, I.P. Parkin, D.R. Williams, Sol–gel synthesis of high-density zeolitic imidazolate framework monoliths via ligand assisted methods: exceptional porosity, hydrophobicity, and applications in vapor adsorption, Adv. Funct. Mater. 31 (2021), 2008357, https://doi.org/10.1002/adfm.202008357.
[24] Y. Zhang, Y. Jia, M. Li, L. Hou, Influence of the 2-methylimidazole/zinc nitrate hexahydrate molar ratio on the synthesis of zeolitic imidazolate framework-8 crystals at room temperature, Sci. Rep. 8 (1) (2018) 1–7, https://doi.org/10.1038/s41598-018-28015-7.
[25] B.J. El Taher, R. Sabouni, M. Ghommem, Luminescent metal organic framework for selective detection of mercury in aqueous media: microwave-based synthesis and evaluation, Colloids Surf. A Physicochem. Eng. Asp. 607 (2020), 125477, https://doi.org/10.1016/j.colsurfa.2020.125477.
[26] Y. Zhang, Y. Jia, L. Hou, Synthesis of zeolitic imidazolate framework-8 on polyester fiber for PM2.5 removal, RSC Adv. 8 (2018) 31471–31477, https://doi.org/10.1039/c8ra06414h.
[27] S. Zhang, et al., Carbonic anhydrase enzyme-MOFs composite with a superior catalytic performance to promote CO 2 absorption into tertiary amine solution, Environ. Sci. Technol. 52 (2018) 12708–12716, https://doi.org/10.1021/acs.est.8b04671.
[28] W.S. Chi, et al., Mixed matrix membranes consisting of SEBS block copolymers and size-controlled ZIF-8 nanoparticles for CO2 capture, J. Membr. Sci. 495 (2015) 479–488, https://doi.org/10.1016/j.memsci.2015.08.016.
[29] C.J. Wijaya, S. Ismadji, H.W. Aparamarta, S. Gunawan, Facile and green synthesis of starfruit-like ZIF-L, and its optimization study, Molecules 26 (2021) 4416.
[30] P. Khanh, N.T. Trung, Understanding interaction capacity of CO2 with organic compounds at molecular level: a theoretical approach, in: Carbon Dioxide Chemistry, Capture and Oil Recovery, 2018.
[31] M. Polisi, et al., CO2 adsorption/desorption in FAU zeolite nanocrystals: in situ synchrotron X-ray powder diffraction and in situ fourier transform infrared spectroscopic study, J. Phys. Chem. C 123 (4) (2019) 2361–2369, https://doi.org/10.1021/acs.jpcc.8b11811.
[32] C. Nieto-draghi, G. Chaplais, A. Simon-masseron, Adsorption of CO2, CH4, and N2 on zeolitic imidazolate frameworks: experiments and simulations, Chem. Eur J. 16 (2010) 1560–1571, https://doi.org/10.1002/chem.200902144.
[33] D. Weibel, Z.R. Jovanovic, E. Gálvez, A. Steinfeld, Mechanism of Zn particle oxidation by H2O and CO2 in the presence of ZnO, Chem. Mater. 26 (22) (2014) 6486–6495, https://doi.org/10.1021/cm503064f.
[34] S.S. Myers, K.R. Wessells, I. Kloog, A. Zanobetti, J. Schwartz, Effect of increased concentrations of atmospheric carbon dioxide on the global threat of zinc deficiency: a modelling study, Lancet Global Health 3 (10) (2015) e639, https://doi.org/10.1016/S2214-109X(15)00093-5. –e645.
[35] S. Namba, A. Takagaki, K. Jimura, S. Hayashi, R. Kikuchi, S. Ted Oyama, Effects of ball-milling treatment on physicochemical properties and solid base activity of hexagonal boron nitrides, Catal. Sci. Technol. 9 (2) (2019) 302–309, https://doi.org/10.1039/c8cy00940f.
[36] M. Pérez-Miana, J.U. Reséndiz-Ordóñez, J. Coronas, Solventless synthesis of ZIF-L and ZIF-8 with hydraulic press and high temperature, Microporous Mesoporous Mater. 328 (2021), 111487, https://doi.org/10.1016/j.micromeso.2021.111487.
[37] A. Mohamed, Co2 Selective Metal Organic Framework Zif-8modified Through Ilencapsulation, A Computational Study, 2018.
[38] A. Deacon, et al., Understanding the ZIF-L to ZIF-8 transformation from fundamentals to fully costed kilogram-scale production, Commun. Chem. 5 (18) (2022), https://doi.org/10.1038/s42004-021-00613-z.
[39] H. Misran, N. Mahadi, S.Z. Othman, Z. Lockman, N. Amin, Room temperature synthesis and characterizations of ZIF-8 formation at water-fatty alcohols interface room temperature synthesis and characterizations of ZIF-8 formation at water-fatty alcohols interface, J. Phys. Conf. Ser. 1082 (2018), 012046, https://doi.org/10.1088/1742-6596/1082/1/012046, 8–14.
[40] B. The Huy, D.T. Thangadurai, M. Sharipov, N. Ngoc Nghia, N. Van Cuong, Y.I. Lee, Recent advances in turn off-on fluorescence sensing strategies for sensitive biochemical analysis - a mechanistic approach, Microchem. J. 179 (March) (2022), 107511, https://doi.org/10.1016/j.microc.2022.107511.
[41] S. Wang, B. Zang, Y. Chang, C. Hongqi, Synthesis and carbon dioxide capture properties of flower-shaped zeolitic imidazolate framework-L, CrystEngComm 10 (2019) 1039.
[42] N. Missaoui, H. Kahri, U.B. Demirci, Rapid room-temperature synthesis and characterizations of high-surface-area nanoparticles of zeolitic imidazolate framework-8 (ZIF-8) for CO2 and CH4 adsorption, J. Mater. Sci. 57 (34) (2022) 1–13.
[43] C. Soodsuansi, S. Kulpratipunja, C. Ratanatawanate, P. Rangsunvigit, Adsorption of methane and carbon dioxide on activated carbon and ZIF-8 (Zeolitic Imidazolate Framework), Chemical Engineering Transactions 70 (2018) 1633–1638, https://doi.org/10.3303/CET1870273.
[44] Q. Liu, et al., Metal-organic frameworks based fluorescent sensor array for discrimination of flavonoids, Talanta 203 (2019) 248–254, https://doi.org/10.1016/j.talanta.2019.05.073.

[45] S.-S. Lee, M. Sharipov, W.J. Kim, Y.-I. Lee, Turn Off–On Fluorescent CO 2 Gas Detection Based on Amine-Functionalized Imidazole-Based Poly(ionic liquid) ," ACS Omega 7 (44) (2022) 40485–40492, https://doi.org/10.1021/acsomega.2c05695.
[46] B. Chocarro-Ruiz, et al., A CO2 optical sensor based on self-assembled metal-organic framework nanoparticles, J. Mater. Chem. A 6 (27) (2018) 13171–13177, https://doi.org/10.1039/c8ta02767f.
[47] meersens,"Indoor air quality: the impact of CO2 on health and well-being at work." https://meersens.com/indoor-air-quality-the-impact-of-co2-on-health-and-wellbeing-at-work/?lang=en..
[48] W. Zhu, X. Li, Y. Sun, R. Guo, S. Ding, Introducing hydrophilic ultra-thin ZIF-L into mixed matrix membranes for CO2/CH4 separation, RSC Adv. 9 (2019) 23390–23399, https://doi.org/10.1039/c9ra04147h.
[49] H.N. Abdelhamid, Removal of carbon dioxide using zeolitic imidazolate frameworks: adsorption and conversion via catalysis, Appl. Organomet. Chem. 36 (8) (2022) e6753.
[50] W.-T. Koo, J.-S. Jang, I.-D. Kim, Metal-organic frameworks for chemiresistive sensors, Chem 5 (8) (2019) 1938–1963, https://doi.org/10.1016/j.chempr.2019.04.013.
[51] L. Yang, et al., Anion pillared metal-organic framework embedded with molecular rotors for size-selective capture of CO 2 from CH 4 and N 2, ACS Sustain. Chem. Eng. 7 (3) (2019) 3138–3144, https://doi.org/10.1021/acssuschemeng.8b04916.
[52] P. Freund, et al., MIL-53(Al)/Carbon films for CO 2 -sensing at high pressure, ACS Sustain. Chem. Eng. 7 (4) (2019) 4012–4018, https://doi.org/10.1021/acssuschemeng.8b05368.
[53] Z. Zhou, et al., A novel bimetallic MIL-101(Cr, Mg) with high CO2 adsorption capacity and CO2/N2 selectivity, Chem. Eng. Sci. 7 (4) (2016) 4012–4018, https://doi.org/10.1016/j.ces.2016.03.035.
[54] W.R. Lee, et al., Exceptional CO2 working capacity in a heterodiamine-grafted metal-organic framework, Chem. Sci. 6 (7) (2015) 3697–3705, https://doi.org/10.1039/c5sc01191d.
[55] Y.L. Wu, et al., Synthesis of two new Cd(II)-MOFs based on different secondary building units with highly selective gas sorption for CO2/CH4 and luminescent sensor for Fe3+ and Cr2O72− ions, J. Solid State Chem. 285 (2020), 121258, https://doi.org/10.1016/j.jssc.2020.121258.
[56] X. Chong, K.J. Kim, P.R. Ohodnicki, E. Li, C.H. Chang, A.X. Wang, Ultrashort near-infrared fiber-optic sensors for carbon dioxide detection, IEEE Sensor. J. 15 (9) (2015) 5327–5332, https://doi.org/10.1109/JSEN.2015.2438063.
[57] M.S. Alivand, M. Shafiei-Alavijeh, N.H.M.H. Tehrani, E. Ghasemy, A. Rashidi, S. Fakhraie, Facile and high-yield synthesis of improved MIL-101(Cr) metal-organic framework with exceptional CO2 and H2S uptake; the impact of excess ligand-cluster, Microporous Mesoporous Mater. 279 (2019) 153–164, https://doi.org/10.1016/j.micromeso.2018.12.033.